

Optimizing Communication for Latency Sensitive HPC Applications on up to 48 FPGAs Using ACCL

Marius Meyer^{1,2}, Tobias Kenter^{1,2}, Lucian Petrica³, Kenneth O'Brien³,
Michaela Blott³, and Christian Plessl^{1,2}

¹ Paderborn University, Department of Computer Science, Warburger Str. 100,
Paderborn, Germany

{marius.meyer, kenter, christian.plessl}@uni-paderborn.de

² Paderborn Center for Parallel Computing, Mersinweg 5, Paderborn, Germany

³ AMD Research, 2020 Bianconi Ave, Dublin, Ireland

{lucian.petrica, ken.obrien, michaela.blott}@amd.com

Abstract. Most FPGA boards in the HPC domain are well-suited for parallel scaling because of the direct integration of versatile and high-throughput network ports. However, the utilization of their network capabilities is often challenging and error-prone because the whole network stack and communication patterns have to be implemented and managed on the FPGAs. Also, this approach conceptually involves a trade-off between the performance potential of improved communication and the impact of resource consumption for communication infrastructure, since the utilized resources on the FPGAs could otherwise be used for computations. In this work, we investigate this trade-off, firstly, by using synthetic benchmarks to evaluate the different configuration options of the communication framework ACCL and their impact on communication latency and throughput. Finally, we use our findings to implement a shallow water simulation whose scalability heavily depends on low-latency communication. With a suitable configuration of ACCL, good scaling behavior can be shown to all 48 FPGAs installed in the system. Overall, the results show that the availability of inter-FPGA communication frameworks as well as the configurability of framework and network stack are crucial to achieve the best application performance with low latency communication.

Keywords: FPGA · HLS · HPC · inter-FPGA Communication

1 Introduction

ACCL [5] is a collective communication library for field programmable gate arrays (FPGAs) offering an MPI-like API for data exchange between multiple FPGAs using a packet-switched network established directly via the QSFP ports of the FPGA boards. These ports allow data transfer with speeds up to 100 GBit/s while open-source network stack implementations of UDP [11] and TCP [4] exist

to transfer data via these ports. Without ACCL, integrating these network stacks into a user design is non-trivial because it requires the user to have detailed knowledge about the network protocol itself and its implementation. Also, it requires implementing common communication patterns from scratch for every project and handling low-level details like IP addresses or network sockets.

ACCL aims to provide a higher level of abstraction by implementing a message-passing interface well-suited for high performance computing (HPC) applications, which is usable within high level synthesis (HLS) FPGA applications. It supports well-established MPI-like communication patterns including point-to-point communication, collectives, and communicators, while abstracting away the underlying network stack and networking details. As a downside, ACCL itself and the network stacks consume additional hardware resources on the FPGA which limits the resources available for the actual application. This introduces a trade-off between single-FPGA application performance and communication latency and throughput, which again may benefit the overall application performance. As a different approach – and on the other side of the discussed trade-off – HPCC FPGA [10] and MVAICH2-FPGA [1] use the host MPI implementation for inter-FPGA communication, avoiding additional FPGA resource utilization, but incurring increased communication latency and limited throughput.

In this work, we evaluate the performance of ACCL and its network stacks for use in multi-FPGA applications and compare it to an implementation using the host-side communication approach discussed in HPCC FPGA [10]. Therefore, we split our work into two parts.

In the first part in Section 3, we will use synthetic benchmarks to measure the differences in resource utilization, communication latency, and throughput for different ACCL configurations and compare them to the communication approach taken by HPCC FPGA. Also, we provide models for communication latency and discuss the limitations and opportunities for different ACCL- and host-based communication approaches. Moreover, we discuss optimization options for ACCL and its network stacks for the inter-FPGA network infrastructure of the Noctua 2 supercomputer, which contains one of the largest installations of FPGAs in the academic HPC domain.

In the second part, in Section 4, we port a multi-FPGA shallow water simulation that operates on unstructured meshes [2] and has strong requirements for low-latency communication to Xilinx FPGAs. We use our findings from Section 3 to identify the best ACCL configuration for this kind of application and evaluate the scaling behavior of the application over up to 48 FPGAs compared to a baseline version using host MPI for communication. In addition, we extend the existing performance models of the shallow water simulation to also reflect communication latency to show the effect of high communication latency on the application scalability.

2 Related Work

This work analyzes ACCL as an inter-FPGA communication framework for scaling latency-sensitive applications. Several multi-FPGA applications exist, using either other existing communication frameworks or custom solutions.

Fujita *et al.* [3] accelerate astrophysical simulations using FPGAs and the inter-FPGA communication framework CIRCUS. They achieve a high parallel efficiency with a weak scaling scenario on up to four FPGAs. Kobayashi *et al.* [8] extends the work utilizing GPUs and FPGAs and using MPI and CIRCUS for communication. The application showed linear speedups for weak scaling on up to two compute nodes or up to two FPGAs, respectively. However, the scaling evaluation for this application is very limited.

Huthmann *et al.* [6] implemented an N-Body simulation using a custom circuit-switched network. The implementation showed linear speedups in strong and weak scaling scenarios over up to 8 FPGAs. Another N-Body simulation by Menzel *et al.* [9] uses SerialLite via the OpenCL Intel External Channel extension to communicate within a custom circuit-switched network and archives linear scaling in a strong scaling scenario with up to 24 FPGAs. The implementation achieves sub-millisecond time step durations.

A shallow water simulation on unstructured meshes by Faj *et al.* [2] similarly makes use of SerialLite within a custom circuit-switched network. The mesh is therefore partitioned and distributed over the FPGAs. FPGAs holding neighboring partitions are directly connected via the custom circuit-switched network for halo exchanges. Because of that, the number of neighboring partitions is limited to the number of available ports on the FPGA board. The implementation is scaled over up to 10 FPGAs and achieves high parallel efficiency in strong scaling scenarios with a time step duration of only several microseconds. These small time steps set high requirements on the communication latency, thus we picked this work for our evaluation.

The HPCC FPGA benchmark suite [10] contains multi-FPGA implementations for LU factorization and matrix transposition. Next to the baseline versions using the naive communication approach via PCIe and MPI, it also contains optimized versions of these benchmarks directly utilizing the SerialLite network stack for communication in custom circuit-switched networks. The LU factorization does not have tight constraints on communication latency or throughput since communication latencies can be hidden by computation for large matrices. The matrix transposition is mainly communication throughput limited. Both applications were executed on up to 25 FPGAs showing close to linear speedups for communication in custom circuit-switched networks.

3 Synthetic Benchmarking of Communication Approaches

3.1 ACCL Communication Approaches

ACCL offers two communication approaches: *streaming* and *buffered* communication. *Buffered* communication is similar to the well-known blocking MPI

communication, whereas *streaming* communication supports the processing of incoming data before the transmission is complete. This allows further overlapping of communication and computation. As additional configuration option, ACCL supports the scheduling of communication from the host side (offering more flexibility), or directly from FPGA.

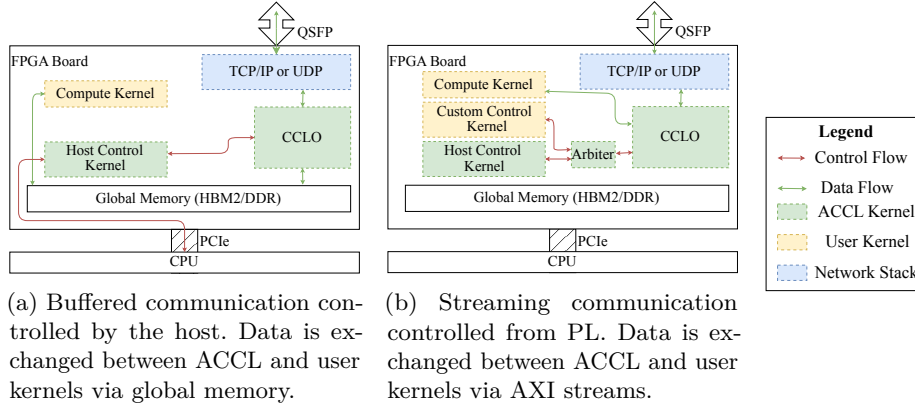


Figure 1: Two examples of communication approaches using the ACCL framework.

Buffered communication with communication scheduling from the host side is visualized in Figure 1a. Here, ACCL will transfer data from a buffer in global memory to another buffer in the global memory of a remote FPGA. The *compute kernel* – the actual application implemented on FPGA – can read the data from this global memory buffer afterwards. The communication is controlled on the host via a C++ library. Instead of exchanging data between the *compute kernel* and the ACCL infrastructure indirectly via global memory, it can also be directly forwarded using AXI streams. This approach is indicated in Figure 1b as a green AXI stream between *compute kernel* and *CCLO*. A drawback of this approach is, that the order of incoming messages can not be controlled by the receiving side because received data is directly forwarded from ACCL to the AXI stream. If two FPGAs stream a message to the same recipient, the contents of the message will be forwarded in the order of arrival, which may also lead to a scattering of messages. The compute kernels need to be extended to handle these situations.

The other configuration option builds upon the AXI stream interface that is used to issue commands. In addition to the default *host control kernel* (Figure 1a) that requires a dedicated kernel invocation for every communication request, it is also possible to implement *custom control kernels* (Figure 1b). ACCL already comes with an API that can be used from HLS kernels to implement this functionality. A *custom control kernel* implements the communication pattern required by a specific *compute kernel* and thus can significantly reduce the number

of required kernel invocations. *Compute kernel* and *custom control kernel* can also be combined into a single kernel.

3.2 Evaluation Infrastructure

For our evaluation, we use the FPGA partition of the Noctua 2 cluster at the Paderborn Center for Parallel Computing (PC²) to synthesize and execute the benchmarks and applications discussed in this paper. Noctua 2 contains one of the largest FPGA installations in the academic HPC domain with a total of 48 Alveo U280 FPGAs distributed over 16 nodes. All FPGAs are connected to an optical switch over their QSFP28 ports as given in Figure 2.

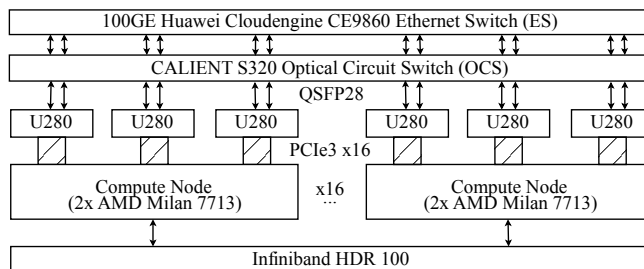


Figure 2: The network infrastructure of the FPGA nodes within the Noctua 2 cluster. The FPGAs are connected to a dedicated Ethernet switch via their QSFP28 ports. The compute nodes communicate via a separate Infiniband network.

The optical switch is protocol agnostic and can be used to physically connect arbitrary ports of the switch to form direct point-to-point connections with minimal latency overhead. In addition, a 128-port ethernet switch is also connected to the optical switch. By configuring the optical switch, this setup also allows the connection of FPGA ports to the ethernet switch to form packet-switched networks. We use this setup in our evaluation to look more deeply into the communication latencies introduced by packet-switched communication. We used Vitis 2022.2, XRT 2.14, and the shell `xilinx_u280_gen3x16_xdma_1_202211_1` for the synthesis and execution of all applications.

3.3 Resource Utilization of the Network Stack

We used the benchmark *b_eff* from the HPCC FPGA [10] benchmarks suite to evaluate the resource utilization of ACCL and the network stack on the FPGA. *b_eff* is a synthetic benchmark where the FPGAs are arranged in a (virtual) ring topology to exchange messages. The messages are sent for a given range of message sizes in a ping-ping fashion between the neighbors in the ring and can be used to measure the latency and throughput of the network.

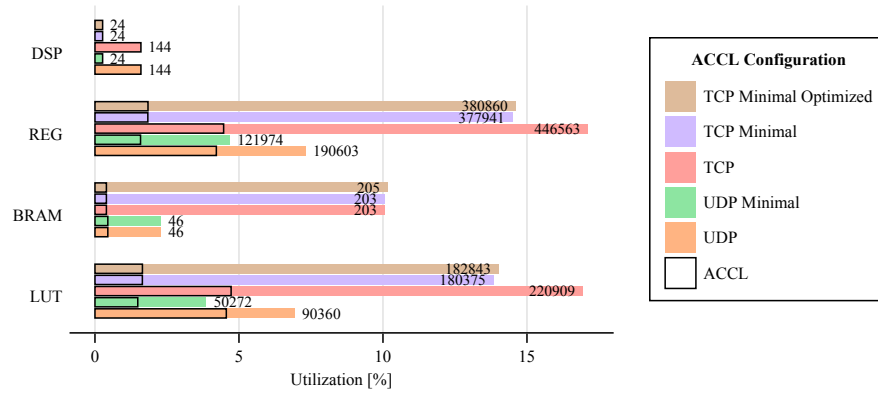


Figure 3: Resource utilization of the network stack and ACCL on the Alveo U280. The ACCL *Minimal* versions do not contain the compression and arithmetic plugins. The resource utilization of ACCL (green boxes in Figure 1) is highlighted by black boxes. All further resources are consumed by the network stack (blue boxes in Figure 1).

We implemented *b_eff* designs with ACCL based on the implementation presented in Figure 1b, now further differentiating between the TCP/IP and the UDP network stack. The resource utilization for different ACCL configurations is given in Figure 3. Further variants are shown, because ACCL is extendable by plugins which are included by default and provide extra functionality for data compression and arithmetic operations used in collectives, such as reductions. These plugins can be removed from the ACCL configuration by setting build flags during synthesis. Since functionality is not needed by *b_eff*, we also synthesized a *minimal* ACCL without unused plugins to save additional resources. Moreover, to optimize the TCP throughput with the Ethernet switch, we synthesized an *optimized* TCP stack configuration. We discuss these optimization steps in more detail in Section 3.4. As expected, the TCP network stack consumes considerably more resources compared to the UDP stack. Our minimal ACCL version saves more than half of the logic resources and more than 83% of DSPs independent of the used network stack.

3.4 Modelling and Measurement of Throughput and Latency

We executed the *b_eff* benchmark for the different communication approaches discussed in Section 3.1 on two FPGAs. For the first experiment, we configured the optical switch to create a direct connection between the FPGAs – bypassing the ethernet switch. Furthermore, the HPCC FPGA version from the original benchmark without ACCL was used to retrieve data for a purely CPU-based baseline. The two FPGAs are located on different nodes, such that data transfers of the baseline version use the Infiniband network of the hosts via MPI.

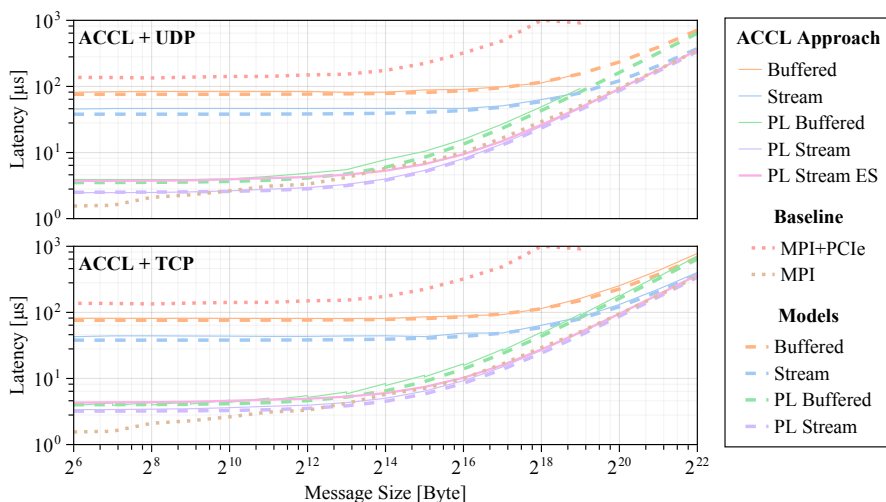


Figure 4: Full-duplex communication latencies using ACCL UDP and TCP network stacks and the discussed communication approaches. The latencies for host-side scheduling are modeled for buffered and streaming communication. Communication via the ethernet switch is marked with ES in the legend. All other measurements are done with directly connected FPGAs.

The communication latencies over the message size are given for *streaming* and *buffered* communication in Figure 4, each in combination with communication scheduling from the host and with a custom control kernel from the FPGA (denoted here as *PL*). We also integrated a performance model for the different approaches as dashed lines in the plot. As expected, the baseline communication approach shows the highest communication latency over all message sizes with latencies of more than $120\mu\text{s}$ for 64 Byte messages. Using the buffered ACCL communication scheduled from the host side, the major limitation for the latency becomes the kernel scheduling time. The ACCL host control kernel needs to be executed two times for sending and receiving a message. We measured around $30\mu\text{s}$ of latency for a single kernel invocation through the used XRT runtime. In contrast, messages scheduled directly from *PL* reach latencies below $3\mu\text{s}$.

We modeled the latency for buffered and streamed communication using the theoretical peak throughput of the involved links as well as our measured kernel start overheads. For buffered communication, this results in the model given in Equation 1, where l_k is the time required to schedule a command to ACCL, l_m the latency to copy the message from the receive buffer in global memory to the destination buffer on the receiving FPGA, and l_c is the latency of the communication link. For host scheduled communication, l_k equals the kernel invocation latency, whereas for *PL* scheduling it is reduced to a fraction of

microseconds since it only represents the time required by ACCL to process the command.

$$2 \cdot l_k + l_m + l_c \tag{1}$$

For streaming, the model simplifies to $l_k + l_c$, because only a single kernel invocation is required per transmission. Also, there is no copy operation required since the data is directly passed to the AXI stream of the user kernel. While l_k is a constant overhead per ACCL command, l_c and l_m depend on the message size and overtake the equation for large message sizes. The additional copy operation required in buffered communication thus leads to a reduced theoretical peak throughput of $(14\text{GB/s}^{-1} + 12.5\text{GB/s}^{-1})^{-1} = 6.6\text{GB/s}$ – only slightly more than half of the peak throughput of the communication link.

Additionally, we compared the communication latency of the network configuration with direct optical links to the latency of connections via the ethernet switch. Overall, the ethernet switch adds around $1\mu\text{s}$ of latency for both network stacks resulting in latencies of 2.5 to 5 μs for small 64 Byte messages. For the TCP stack, the throughput was at first considerably reduced when using the Ethernet switch. Because of the increased communication latency, the sending side has to stop transmission and wait for acknowledgments. In our optimized TCP implementation, we enabled window scaling to overcome this issue, with a minor impact on resource consumption as shown in Section 3.3. Moreover, we reduced the overall protocol overhead by enabling jumbo frames on the Ethernet switch and increasing the maximum segment size for the TCP stack and the maximum packet size in the ACCL firmware accordingly. These changes increased the throughput for large messages from initially 8.5 GB/s with the TCP stack to 12.3 GB/s for both network stacks while having no measurable impact on the latency for small messages. The measurements via the ethernet switch for the optimized TCP and UDP stack are also given in Figure 4 and annotated with *ES*.

4 Acceleration of Shallow Water Simulation using ACCL

4.1 Implementation

The evaluation of ACCL using synthetic benchmarks showed that low latency communication in the order of a few μs is possible. We applied the lessons learned to a full FPGA accelerated HPC application: A discontinuous Galerkin shallow water simulation on unstructured meshes which was originally implemented for Intel FPGAs [7] and was further extended for multi-FPGA execution in custom circuit-switched communication networks [2].

The tidal flow of the bight of Abaco on Bahamas islands is used as a simulation scenario as given in Figure 5. The water surface of the bay is represented by an unstructured mesh. The borders of the mesh are either land or sea edges which have to be handled differently in the simulation. For the execution over multiple FPGAs, the mesh is partitioned into sub-meshes as visualized in Figure 6. The

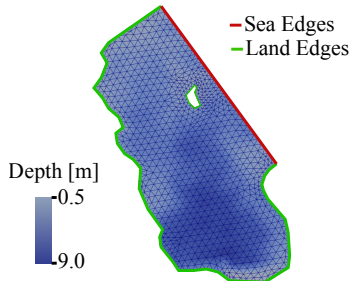


Figure 5: Computational mesh consisting of 1696 elements [2]. The boundary edges represent the coastline (land edges) and the border to the open sea (sea edges).

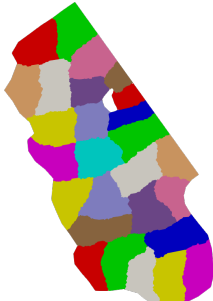


Figure 6: The mesh is partitioned as indicated by the colors. Data has to be exchanged between neighboring partitions in every simulation time step.

mesh partitions are distributed among the FPGAs, such that every FPGA handles exactly one partition. In each simulation step, the halo around the partition edges has to be exchanged between neighboring FPGAs using point-to-point communication. The designs in [7] and [2] support three types of polynomial discontinuous Galerkin discretizations, however, it has been shown by Faj et al. [2] that the requirements for communication latency are very similar for all three types of discretization. Thus, we will only focus on the piecewise constant discretization in our evaluation.

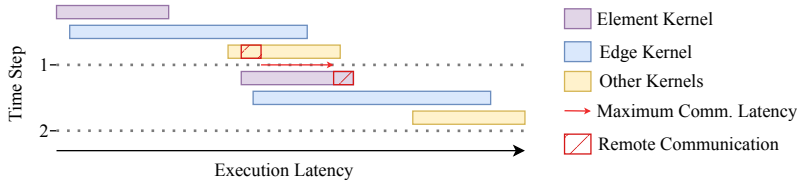


Figure 7: Dataflow schematic for shallow water simulation. Full overlap of compute kernels across simulation time steps. The maximum communication latency is indicated by the red arrow. If communication takes longer, the compute pipeline will stall until data is received. Simplified dataflow based on Faj *et al.* [2], Fig. 5

Figure 7 shows the dataflow graph over two simulation time steps for the compute pipeline in a single FPGA. All simulation data is loaded into the local memory of the FPGA at the beginning of the simulation so global memory

accesses are only used during simulation to write back intermediate results. The *element kernel* updates all entities of the unstructured mesh element-wise. The L^2 projection is directly forwarded to the *edge kernel* which will update all boundary and outer edges of the unstructured mesh. Afterwards, the boundary edges between partitions of the unstructured mesh will be sent within the *other kernels* to the remote FPGAs via ACCL. This data will be received at the end of the execution of the *element kernel* in the next time step. To prevent pipeline stalls, the data has to arrive at the remote FPGA within the latency indicated by the red arrow which is typically a few thousand clock cycles. The overall latency between sending and receiving boundary elements depends mainly on the number of core elements that will be updated by the *element kernel* in between. Core elements are elements that are not located on a border of the local partition and which do not require any data from remote FPGAs.

The data is streamed through the kernels element-wise as given in Figure 8. The mesh partition will be updated on the local FPGA and all boundary elements are forwarded to a *communication kernel* which has the task of passing this data to the compute pipeline on the remote FPGA. In the baseline implementation, the *communication kernel* is invoked by the host for every simulation step. It will write all received data into a buffer in global memory and finish execution after all elements for one simulation step are written to notify the host that the data is ready for sending via MPI. The remote host calls the *communication kernel* again to read the data from global memory to the *element kernel* for the next simulation step.

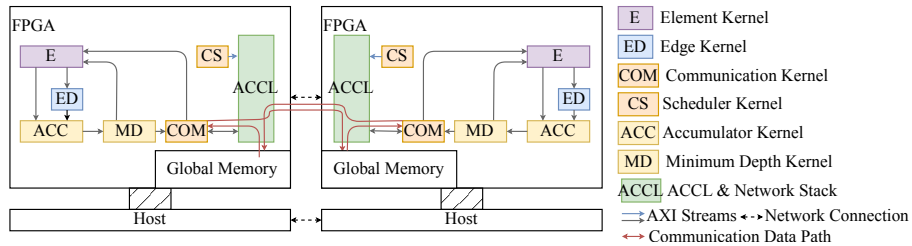


Figure 8: Remotely partitioned FPGA designs with two processing pipelines distributed over two FPGAs with ACCL communication via AXI streams and communication scheduling in PL.

For the ACCL-enabled version, the *communication kernel* converts the simulation data into a generic 512-bit AXI stream used to directly pass the data into the ACCL communication stack. This way, the actual simulation loop stays unchanged. In addition, we use a communication scheduler kernel to issue the send and receive commands directly from PL. This massively reduces the number of kernel invocations from the host side.

For a high number of partitions, there will be more than one neighboring partition and the *element kernel* expects the remote elements from the communication kernel in a predefined order. As a result, the incoming data has to be reordered on the receiver side before it can be passed onto the simulation pipeline. Instead of creating our own logic for this task, we make use of ACCL’s buffered communication feature. Therefore, we buffer received data in global memory first and move the data from the global memory into the AXI stream using the `recv` primitive as indicated by the red arrows in the figure. In the end, the resulting communication scheme is a mixture of streaming communication on the sending side and buffered communication on the receiving side. This approach slightly increases the communication latency because data has to go through the global memory instead of passing it directly to the communication kernel. As a main advantage, we have no strict upper limit for the number of neighboring partitions since we can configure the number of receive buffers during runtime.

4.2 Performance Model

The port of the simulation to Vitis-compatible C++ code was possible without major changes in the dataflow characteristics. This also means, that the performance models for the simulation proposed by Faj *et al.* [2] also hold for this implementation. However, their throughput model does not consider the communication latency, which is important for strong scaling scenarios and small local partition sizes, since the calculations on the core elements may not be sufficient to hide the communication latency. Because of this, we extended the existing throughput model as given in Equation 2 with the communication latency L_{comm} representing the latency for the FPGA with the highest number of neighbors according to the partition scheme and the largest number of sent or received elements per simulation time step.

$$throughput = f \cdot \frac{FLOP_{total}}{\max(E_{core} + D_{ext}, L_{comm}) + E_{send} + E_{recv} + L_{pipe}} \quad (2)$$

Additionally, we model the communication latency based on our latency measurements in Section 3, our ACCL latency models, as well as mesh partitioning information as given in Equation 3. As described in the previous section, to receive the data, it has to be read from a buffer in global memory with a latency of l_m . The maximum number of neighbors N_{max} for a partition scheme has a major effect on this read latency because the read commands have to be scheduled for every neighbor. This adds l_m to the overall communication latency for every neighbor as given in Equation 1. The latency to process the commands in ACCL l_k has to be added for every send and receive command.

$$L_{comm} = \frac{E_{send} + E_{recv} + 2 \cdot N_{max} \cdot l_k + N_{max} \cdot l_m}{f} + L_{pingping} \quad (3)$$

Also, the overall latency of the communication link has to be considered, introducing another latency $L_{pingping}$, which is the ping-ping latency of the largest

message exchanged among neighbors. For the total number of floating-point operations $FLOPS_{total}$ we use the simplified model $FLOPS_{total} = FLOP_{sum} \cdot E_{total}$ without the additional operations required to calculate the projection on the received elements. Instead, we calculate the FLOPs based on the total number of elements in the mesh E_{total} and the number of floating point operations per element $FLOPS_{sum}$, independent of the partitioning to make scaling experiments better comparable.

4.3 Evaluation

We synthesized the base and ACCL version of our shallow water simulation for the same infrastructure described in Section 3.2. For our application, we use the UDP minimal and TCP minimal optimized configurations of ACCL as described in Section 3.3. The resulting resource utilization is given in Table 1 for the used configurations. The increased resource utilization compared to the base version closely reflects the resource usage of the ACCL stack. The implementation supports setting the maximum number of elements per partition, which mainly affects the BRAM and URAM utilization since the whole partition is stored in local memory. The baseline and UDP versions are synthesized with a partition size of 8192 elements where larger sizes led to routing congestion because the URAMs holding the local partition can not be easily distributed across multiple sliced logic regions (SLRs). For the ACCL TCP stack, we were only able to synthesize designs with half the partition size, i.e. 4096 elements. Larger local partitions also failed because of routing congestion.

Table 1: Resource utilization of the shallow water simulation

Configuration	LUTs	Registers	BRAM	URAM	DSPs	Freq. [MHz]	Synth. Time [h]
Base	126,646 (9.7%)	182,015 (7.0%)	265 (13.1%)	188 (19.6%)	1,218 (13.5%)	256	4.1
ACCL UDP	176,884 (13.6%)	305,381 (11.7%)	312 (15.5%)	188 (19.6%)	1,242 (13.8%)	274	5.2
ACCL TCP	334,225 (25.6%)	586,847 (22.5%)	344 (17.1%)	101 (10.5%)	1,242 (13.8%)	252	15.1

We first executed a weak scaling experiment with the three design variants of the shallow water simulation. The resulting performance compared to the modified performance model is given in Figure 9. We used increasing mesh sizes with up to 312,000 elements to keep the number of elements per partition between 6,000-7,000 elements. The base version annotated as *MPI+PCIe* first shows a reduced performance when scaling from one partition to two partitions. When executed only on one partition, no communication is required, eliminating compute pipeline stalls. Measurements with our synthetic benchmark given in Figure 4 showed an expected latency of 100-120 μ s for small messages of multiple KB size. This is the expected size of the halo exchange messages sent by the shallow water simulation. The simulation processes one element per clock cycle and sufficient core elements are required to hide the communication latency as

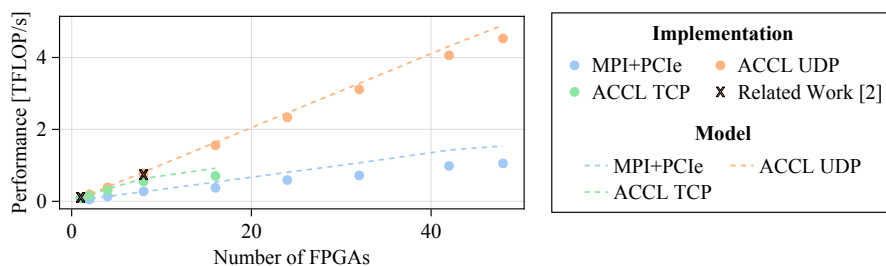


Figure 9: Execution times for the weak scaling scenario with ~ 6000 elements per FPGA. Due to a known issue in the current version of the TCP stack, we did not evaluate this configuration beyond 16 devices.

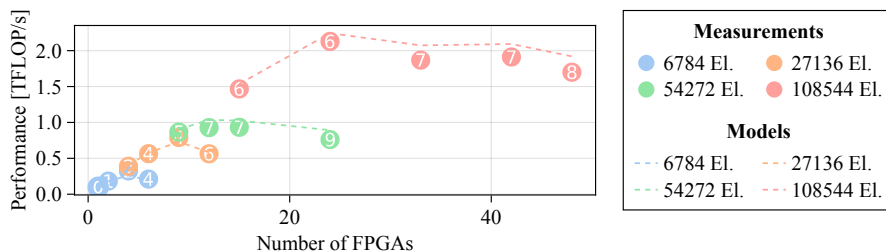


Figure 10: Strong scaling scenario with selected mesh sizes with ACCL and UDP stack. The numbers in the plot represent the maximum number of neighbors.

expressed in the max term in Equation 2. Based on the kernel frequency of the synthesized bitstream, the pipeline could process around 25,000 to 30,000 elements in this time frame, so for the given partitions, the pipeline stalls approximately 75-80% of the execution time. With their improved communication latency, the ACCL designs with UDP and TCP stack can respectively avoid or reduce such stalls, which leads to higher performance and better scalability, to up to 4.5 measured TFLOPs on 48 FPGAs with the ACCL UDP design.

Furthermore, we executed strong scaling experiments with selected mesh sizes given in Figure 10, which additionally depict the maximum number of communication neighbors. The results show that this number has a high impact on the overall performance, because of the additional latency introduced by command scheduling and global memory. When the local partitions become too small to cover the communication latency, there is no performance improvement by adding further FPGAs. Indeed, the overall performance can even degrade, because further partitioning of the mesh may introduce a higher maximum number of neighbors, which in turn further increases the communication latency. This can be clearly observed for the 108K element mesh, where additional neighbors result in a step-wise decrease in performance. The original implementation of [2] is limited to a maximum of four neighbors because of the number of QSF

ports installed on the FPGA board and thus was limited to at most 10 FPGAs for the topology used in their and our experiments. Our ACCL implementation overcomes this limitation, but we see that in strong scaling scenarios, larger local partition sizes or custom message reordering in local memory would be required to hide the communication overheads introduced by the increasing number of neighbors.

5 Conclusion

In this work, we modeled the communication latency with ACCL for buffered and streamed communication and showed, that buffered communication leads to latency and throughput degradation because of additional copy operations. Also, communication scheduling from PL was shown to drastically improve communication latency because of a reduced number of kernel invocations. Based on our ACCL evaluation, we ported a multi-FPGA shallow water simulation to Xilinx FPGAs and extended it with communication via ACCL. The scaling experiments showed linear speedups in weak scaling scenarios with all 48 FPGAs of the Noctua 2 partition and the same performance per partition, but with much better scalability than an implementation using custom circuit-switched networks. This makes ACCL and packet-switched network infrastructures good candidates for scaling communication-latency-sensitive multi-FPGA applications.

Acknowledgements The authors gratefully acknowledge the computing time provided to them on the high-performance computer Noctua 2 at the NHR Center PC2. These are funded by the Federal Ministry of Education and Research and the state governments participating based on the resolutions of the GWK for the national high-performance computing at universities (www.nhr-verein.de/unsere-partner). Also, they thank Markus Büttner and Jonathan Schmalfuss from the University of Bayreuth for the help with mesh generation for the shallow water simulation.

This work was supported in part by AMD under the Heterogeneous Accelerated Compute Clusters (HACC) program. AMD, the AMD Arrow logo, Alveo™, Vitis™, Xilinx and combinations thereof are trademarks of Advanced Micro Devices, Inc. Other product names used in this publication are for identification purposes only and may be trademarks of their respective companies.

References

1. Contini, N., Ramesh, B., Kandadi Suresh, K., Tran, T., Michalowicz, B., Abduljabbar, M., Subramoni, H., Panda, D.: Enabling Reconfigurable HPC through MPI-based Inter-FPGA Communication. In: Proceedings of the 37th International Conference on Supercomputing, pp. 477–487 (2023)
2. Faj, J., Kenter, T., Faghih-Naini, S., Plessl, C., Aizinger, V.: Scalable multi-FPGA design of a discontinuous Galerkin shallow-water model on unstructured meshes. In: Proceedings of the Platform for Advanced Scientific Computing Conference, pp. 1–12 (2023)

3. Fujita, N., Kobayashi, R., Yamaguchi, Y., Boku, T., Yoshikawa, K., Abe, M., Umemura, M.: OpenCL-enabled Parallel Raytracing for Astrophysical Application on Multiple FPGAs with Optical Links. In: 2020 IEEE/ACM International Workshop on Heterogeneous High-performance Reconfigurable Computing (H2RC), pp. 48–55 (2020). <https://doi.org/10.1109/H2RC51942.2020.00011>
4. He, Z., Korolija, D., Alonso, G.: EasyNet: 100 Gbps Network for HLS. In: 2021 31st International Conference on Field-Programmable Logic and Applications (FPL), pp. 197–203. IEEE Computer Society, Los Alamitos, CA, USA (2021). <https://doi.org/10.1109/FPL53798.2021.00040>. <https://doi.ieeecomputersociety.org/10.1109/FPL53798.2021.00040>
5. He, Z., Parravicini, D., Petrica, L., O'Brien, K., Alonso, G., Blott, M.: ACCL: FPGA-Accelerated Collectives over 100 Gbps TCP-IP. In: 2021 IEEE/ACM International Workshop on Heterogeneous High-performance Reconfigurable Computing (H2RC), pp. 33–43 (2021). <https://doi.org/10.1109/H2RC54759.2021.00009>
6. Huthmann, J., Shin, A., Podobas, A., Sano, K., Takizawa, H.: Scaling Performance for N-Body Stream Computation with a Ring of FPGAs. In: Proceedings of the 10th International Symposium on Highly-Efficient Accelerators and Reconfigurable Technologies. HEART '19. Association for Computing Machinery, Nagasaki, Japan (2019). <https://doi.org/10.1145/3337801.3337813>. <https://doi.org/10.1145/3337801.3337813>
7. Kenter, T., Shambhu, A., Faghih-Naini, S., Aizinger, V.: Algorithm-hardware co-design of a discontinuous Galerkin shallow-water model for a dataflow architecture on FPGA. In: Proceedings of the Platform for Advanced Scientific Computing Conference, pp. 1–11 (2021)
8. Kobayashi, R., Fujita, N., Yamaguchi, Y., Boku, T., Yoshikawa, K., Abe, M., Umemura, M.: GPU-FPGA-Accelerated Radiative Transfer Simulation with Inter-FPGA Communication. In: Proceedings of the International Conference on High Performance Computing in Asia-Pacific Region. HPC Asia '23, pp. 117–125. Association for Computing Machinery, Singapore, Singapore (2023). <https://doi.org/10.1145/3578178.3578231>. <https://doi.org/10.1145/3578178.3578231>
9. Menzel, J., Plessl, C., Kenter, T.: The Strong Scaling Advantage of FPGAs in HPC for N-Body Simulations. *ACM Trans. Reconfigurable Technol. Syst.* **15**(1) (2021). <https://doi.org/10.1145/3491235>. <https://doi.org/10.1145/3491235>
10. Meyer, M., Kenter, T., Plessl, C.: Multi-FPGA Designs and Scaling of HPC Challenge Benchmarks via MPI and Circuit-switched Inter-FPGA Networks. *ACM Transactions on Reconfigurable Technology and Systems* **16**(2), 1–27 (2023). <https://doi.org/10.1145/3576200>. <https://dl.acm.org/doi/10.1145/3576200> (visited on 03/29/2023)
11. XUP Vitis Network Example (VNX), https://github.com/Xilinx/xup_vitis_network_example (visited on 07/19/2023)